Quasiclassical state to state reaction cross sections for D+H2(v=0, j=0)→HD(v',j')+H. Formation and characteristics of shortlived collision complexes

F. J. Aoiz, V. J. Herrero, and V. Sáez Rábanos

Articles you may be interested in

Measurement of the statespecific differential cross section for the H+D2→HD(v'=4, J'=3)+D reaction at a collision energy of 2.2 eV
J. Chem. Phys. 103, 5157 (1995); 10.1063/1.470604

Quantum mechanical and quasiclassical calculations for the H+D2→HD+D reaction: Reaction probabilities and differential cross sections
J. Chem. Phys. 101, 5781 (1994); 10.1063/1.467362

Classical collision complexes in the D+H2(v=0, j=0)→HD(v', j')+H reaction
J. Chem. Phys. 95, 7767 (1991); 10.1063/1.461350

Crossed molecular beams study of the reaction D+H2→DH+H at collision energies of 0.53 and 1.01 eV
J. Chem. Phys. 93, 5719 (1990); 10.1063/1.459566

Comparison of quasiclassical trajectory calculations to accurate quantum mechanics for statetostate partial cross sections at low total angular momentum for the reaction D+H2→HD+H
J. Chem. Phys. 91, 1038 (1989); 10.1063/1.457227

Quasiclassical state to state reaction cross sections for D+H$_2$(v=0, j=0)→HD(v′,j′)+H. Formation and characteristics of short-lived collision complexes

F. J. Aoiz
Departamento de Química Física, Facultad de Química, Universidad Complutense, 28040 Madrid, Spain

V. J. Herrero
Instituto de Estructura de la Materia (CSIC), Serrano 123, 28006 Madrid, Spain

V. Sáez Rábanos
Departamento de Química General y Bioquímica, ETS Ingenieros de Montes, Universidad Politécnica, 28040 Madrid, Spain

State resolved total and differential reaction cross sections, as well as reaction probabilities, have been calculated by the quasiclassical trajectory (QCT) method for the D+H$_2$(v=0, j=0)→HD(v′,j′)+H reaction on the Liu–Siegbahn–Truhlar–Horowitz potential energy surface in the collision energy range 0.30–1.25 eV. Thus a detailed comparison with existing fully converged quantum mechanical (QM) calculations has been performed. The general agreement between both sets of results is good with some differences. QCT integral reaction cross sections for the production of HD(v′=0) are lower than the corresponding QM ones by 10%–15% for collision energies higher than 0.6 eV, and the energy dependence of the QCT reaction probability with a total angular momentum J equal to zero shows no structure when summed over all j′ states (contrary to the QM case). The differential cross sections for the lowest j′ values show, when represented as a function of energy, a "ridge" feature similar to the one found in exact QM calculations and attributed to a broad resonance. The analysis of the trajectories leading to low j′ shows progressively longer collision times as the scattering angle decreases. The longest-lived trajectories, related to the formation of short-lived complexes, cause local maxima in the differential cross section at the lowest scattering angles for each energy. These local maxima are the origin of the ridge. The lifetime of the classical short-lived complexes is estimated to be 15–35 fs, clearly larger than the lifetimes obtained from the width of the ridge feature, when interpreted as a quantum mechanical resonance.

I. INTRODUCTION

The possible formation of short-lived complexes in the course of H+H$_2$ reactive encounters is currently attracting a great deal of attention. Complexes of that kind should originate resonances in reactive scattering and the experimental detection of such resonances would be a most sensitive probe of the potential energy surface (PES) in the transition state region. The energies of these resonances correspond to those of the eigenstates of the three atomic complex, and their widths are a measure of the lifetimes of these quasibound states.

The prototype H+H$_2$ reaction is indeed the most appropriate one for the theoretical study of scattering resonances, since it is the only one for which exact quantum mechanical (QM) calculations[1] have been performed on an accurately known PES[2,3] and for a range of initial conditions adequate for the comparison with experimental measurements.[4,5]

On the other hand, the feasibility of exact QM calculations offers a unique opportunity for the comparison with the results from classical mechanics, helping thus to establish the limits of validity of the quasiclassical trajectory (QCT) approach and allowing in principle the identification of quantum mechanical effects in the dynamics.

Dynamical resonances in H+H$_2$ reactive collisions were observed long ago by Truhlar and Kuppermann[6] and by Wu and Levine[7] in quantum calculations for the collinear case. They obtained sharp features in the evolution of the reaction probalility with energy. Later work by Schatz and Kuppermann[8] showed that the resonance structure was present also in the three dimensional (3D) calculations for low values of the total angular momentum (J =0,1). The authors suggested that this resonance structure in the integral cross section could survive the partial wave (J) summation necessary to make the theoretical results comparable with experiments. Subsequent work by Schatz[9] concluded, however, the contrary. This conclusion was confirmed by the results of the fully converged quantum mechanical (QM) calculations by Zhang and Miller[10] on the Liu–Siegbahn–Truhlar–Horowitz (LSTH) surface.[2]

Experimental measurements by Nieh and Valentini[11] on the H+H$_2$ (para) →H$_2$ (ortho) +H reaction, where the H atoms were produced by tunable ultraviolet laser photodissociation of HI and the H$_2$(v′=1,j′) product was detected by means of coherent anti–Stokes Raman spectroscopy (CARS), gave sharp variations in the product yield as a function of collision energy that were assigned to resonances related to states of the H$_3$ complex. Later work by Phillips, Levene, and Valentini[12] also seemed to indicate

the finding of resonance structure in the $D + H_2 \rightarrow HD + H$ system.

These unexpected data led thus to an interesting controversy and stimulated further theoretical and experimental work. Several groups performed rigorous quantum mechanical calculations with different mathematical methods on the $H + H_2 \rightarrow H_2 + H$ (Refs. 13–16) and $D + H_2 \rightarrow HD + H$ (Refs. 17–19) reactions, using the two most accurate potential energy surfaces available.[2,3] The results confirmed the previous theoretical calculations, ruling out the presence of resonances in the integral cross section.

Ultimately, experimental measurements by Kliner, Adelman, and Zare[20] using resonance-enhanced multiphoton ionization (REMPI) for the detection of the $H_2(v'j')$ product have revealed no sharp resonance features in the evolution of the integral cross section with energy, and are in very good agreement with the theoretical predictions.

It is now generally accepted that the dynamical resonances in $H + H_2$ should not be manifest in the dependence of the integral cross section with energy. Nevertheless, a recent analysis by Continetti, Zhang, and Miller[21] and by Miller and Zhang[22] has shown that a structure, possibly due to a "broad" resonance (i.e., with contributions of several J for each resonant energy) can indeed be observed in the energy dependence of the differential state to state (i.e., $v'j'$ resolved) cross section for low j'. The structure attributed to the resonance is clearly seen in a three dimensional plot of the cross section as a function of the center of mass scattering angle θ and of the total energy E, where it takes the form of a "ridge" along a line in the $E-\theta$ plane that moves from backward scattering (with respect to the incoming atom) at low energy to forward scattering at higher energy. In their analysis, the authors related this ridge to a corresponding one in the opacity function $P(J,E)$, and estimated the rotational constant of the three atomic complex.

Muga and Levine[23] proposed a classical mechanism by which collisions with high impact parameter could lead to the formation of a complex, due to the characteristics of the H_3 potential. They stress the plausibility of this mechanism by demonstrating the existence of relatively long-lived ("trapped") trajectories for $H + H_2$ at the energy of the first resonance reported by Valentini.[5] However, the authors do not comment explicitly on the influence of these trapped trajectories in the value of the cross section. Miller has reasonably argued[1] that, whatever their effect may be, it should not appear in the integral cross section, since the range of conditions of the calculations of Muga and Levine is also contained in the exact quantum mechanical results.

Recently, Aoiz, Herrero, and Sáez Rábanos[24] have reported results of quasiclassical trajectory (QCT) calculations for $D + H_2(v=0, j=0) \rightarrow HD(v'=0,j') + H$ that exhibit a ridge structure in the differential cross sections and opacity functions similar to the one found by Miller, Zhang, and Continetti,[21,22] albeit less marked. Trajectories leading to HD products in the ridge are shown to be longer-lived than the rest (though not properly "trapped").

Most interesting is the possibility that the ridge struc-

ture just described is in principle accessible to experiment. Angular distributions with time of flights (TOF) analysis of the products have been measured for this reaction.[25,26] However, the resolution was not good enough to separate the contributions of individual vibrorotational states. More recently, Welge and co-workers[27] have developed a novel method of high resolution for detecting H atoms in Rydberg states, and they can obtain fully vibrational and rotational state resolved product distributions as a function of laboratory scattering angle for the $H + D_2$ reaction. From these measurements, detailed state resolved differential cross sections can be derived that allow a direct comparison with theoretical predictions. On the other hand, Vraking, Bracker, and Lee[28] have devised an experimental setup to study $D + H_2 \rightarrow HD + H$ collisions in crossed molecular beams. For the detection of the HD product they use resonance enhanced multiphoton ionization (REMPI) and a position sensitive ion detector. This scheme should allow the simultaneous measurement of the scattering angle and the internal state $(v'j')$ of the HD molecules produced in the reaction, and should thus enable the experimental investigation of the predicted ridge structure in the differential cross section.

In this work we present extensive QCT calculations followed by careful analysis of the results for the $D + H_2(v=0, j=0) \rightarrow HD(v'j') + H$ reaction, covering the range of energies of interest for the detailed comparison with existing exact quantum mechanical results and with the possible angle and state selective experiments just commented on. In particular, we pay attention to the nature (either pure quantum mechanical or also classical) of the different structures appearing in the cross section calculations, relate some of these structures to the existence of classical short-lived collision complexes (lasting for a fraction of a rotational period of the triatom), and discuss the characteristics and mechanism of formation of these complexes.

II. METHOD

The QCT calculation methodology is basically the same as described in previous work.[29–31]

All the trajectories have been calculated on the LSTH PES[2] and restricted to $v=0$, $j=0$ initial H_2 state. Integration algorithms and tests of accuracy are as reported in Ref. 31. With a step size of 5×10^{-17} s, conservation of total energy and angular momentum were better than 1 in 10^6 and 1 in 10^7, respectively. In order to have a fine grid to calculate the energy dependence of the $v'j'$ state resolved differential cross section, the collision energy is swept from 0.30–1.25 eV in intervals of 0.05 eV, and batches of 20 000–60 000 trajectories were run for each energy. Total number of trajectories calculated in this range was of ca. 8×10^5.

Additional 5×10^4 trajectories have been calculated in the same range of collision energies for zero initial orbital (and hence total) angular momentum. Energies were chosen randomly in each subinterval, but in order to improve the accuracy at the lowest energies, stratified sampling was used.

Assignement of final quantum numbers is done as in previous works by equating the internal energy for a given HD rotational angular momentum to the full Dunham expansion of vibrorotational energies of the HD molecule. The values of v' and j' found in this way are then rounded to the nearest integer. Other assignment schemes allowing a trajectory to contribute to several vibrorotational numbers, as the quadratic smooth sampling procedure,[32] have been tested in several cases, but the results were always indistinguishable within the statistical uncertainties from the simplest histogram assignation.

The reactivity and final state probability density functions, such as the reaction probability as a function of the total energy or orbital angular momentum, solid angle differential cross section, distribution of rotational polarization angles, final state energy distributions, etc., are calculated by the method of moments expansion in Legendre polynomials. Following Ref. 30, Legendre polynomials were preferred to Fourier series,[31,33] since the calculated coefficients have a direct physical meaning.[34] In any case, comparison of the resulting fits obtained by expansion in different polynomial series are almost invariably identical and also in very good agreement with the more common histogram representation.

Since accounts of the procedure have been given elsewhere,[30,31,33] only a brief summary of general character will be presented here with the final expressions for several distributions.

Let x be a reduced (random) variable defined on $-1 \leqslant x \leqslant 1$, and $g(x)$ its probability density function normalized to one. The expression of $g(x)$ in series of Legendre polynomials truncated in the Mth term will be

$$g(x) \sim \frac{1}{2} + \sum_{n=1}^{M} a_n P_n(x), \tag{1}$$

where $P_n(x)$ is the n-degree Legendre polynomial. The coefficients a_n are calculated as the Monte Carlo average

$$a_n = \frac{2n+1}{2} \frac{1}{S_{N_\alpha}} \sum_{i=1}^{N_R} w_i P_n(x_i), \tag{2}$$

where the $(2n+1)/2$ factor arises from the normalization of the $P_n(x)$ and the w_i are the weights of each individual trajectory in the general case where biased sampling is assumed. The sum of the weights of the trajectories contributing to a specific final state α is

$$S_{N_\alpha} = \sum_{i=1}^{N_R} w_i, \tag{3}$$

where the sum extends in general to N_R, the total number of reactive trajectories. When the sampling is unbiased the weights are either $w_i = 1$ or 0 (depending on whether the trajectory ends in α or not) and $S_{N_\alpha} = N_\alpha$ is the number of reactive trajectories in final state α.

The expression of the estimate of the error of the coefficients is easily found to be

$$\gamma_n^2 \equiv \mathrm{var}[a_n] = S_{N_\alpha}^{-1} \left[\left(\frac{2n+1}{2} \right)^2 \langle P_n^2 \rangle - a_n^2 \right] \tag{4}$$

and the error of the series is given by

$$\mathrm{var}[g(x)] = \sum_{n=1}^{M} \gamma_n^2 P_n^2(x). \tag{5}$$

Depending on the specific reactivity function or final state distribution the meaning of x is different. Only a few cases will be considered in what follows, stating their corresponding expressions.

(a) Reaction probability as a function of the total energy at a fixed total angular momentum, $P_r(E;J)$, $\mathbf{J} = \mathbf{L} + \mathbf{J}$. The reduced variable will be given by

$$x = \frac{2E - E_2 - E_1}{\Delta E}, \tag{6}$$

where E_1, E_2 define the range of energies, $\Delta E = E_2 - E_1$, where trajectories are calculated

$$P_r(E;J) \equiv P_r(E) = \frac{2}{\Delta E} Q \, g[x(E)], \tag{7}$$

where Q is the Monte Carlo estimate of the integral

$$Q = \langle P(E) \rangle \Delta E = \int_{E_1}^{E_2} P_r(E) dE \approx \Delta E \frac{S_{N_\alpha}}{N}, \tag{8}$$

where N is the total (reactive and nonreactive irrespective of the final state) number of trajectories, and, as before, S_{N_α} is the sum of the weights of the trajectories with contributions to the final state α.

The error in $P_r(E)$ is given by the square root of the variance, given by

$$\mathrm{var}[P_r(E)] = \left(\frac{N - S_{N_\alpha}}{S_{N_\alpha} N} \right) [P_r(E)]^2 + \left(\frac{2 S_{N_\alpha}}{N} \right)^2 \mathrm{var}[g(x)]. \tag{9}$$

(b) Reaction probability at a fixed energy as a function of the orbital angular momentum L or as a function of the impact parameter.

$$x = \frac{2L(L+1)}{L_{max}(L_{max}+1)} - 1 = \frac{2b^2}{b_{max}^2} - 1, \tag{10}$$

where the assumed correspondence is $L(L+1)\hbar^2 = 2\mu E_T b^2$, $L_{max}(b_{max})$ is the maximum orbital angular momentum (impact parameter) giving rise to reaction into the specific final state, and μ is the $D - H_2$ reduced mass. The reaction probability at L is given by

$$P_r(L) = \frac{4\mu E_T \sigma_R}{\pi \hbar^2 L_{max}(L_{max}+1)} g[x(L)] \tag{11}$$

and

$$P_r(b) = \frac{2\sigma_R}{\pi b_{max}^2} g[x(b)], \tag{12}$$

where σ_R, the reaction cross section for the specific final channel, is evaluated as usual as

$$\sigma_R = \frac{\pi \hbar^2}{2\mu E_T} \int_0^{L_{max}} (2L+1) P_r(L) dL \approx \pi b_{max}^2 \frac{S_{N_\alpha}}{N}. \tag{13}$$

The variance is given by

$$\text{var}[P_r(L)] = \left(\frac{N - S_{N_\alpha}}{NS_{N_\alpha}}\right)[P_r(L)]^2 + \left(\frac{2\sigma_R}{\pi b_{max}^2}\right)^2 \text{var}[g(x)].$$

(14)

(c) Solid angle differential cross section. In this case $x = \cos\theta$, θ the scattering angle,

$$\frac{d^2\sigma_R}{d\omega} = \frac{\sigma_R}{2\pi}g(x)$$

(15)

and

$$\text{var}\left[\frac{d^2\sigma_R}{d\omega}\right] = \left(\frac{N - S_{N_\alpha}}{NS_{N_\alpha}}\right)\left[\frac{d^2\sigma_R}{d\omega}\right]^2 + \left(\frac{\sigma_R}{2\pi}\right)^2 \text{var}[g(x)],$$

(16)

with $\text{var}[g(x)]$ given by Eq. (5).

(d) Distribution of product rotational polarization angles. The angle of polarization χ is given by $\cos\chi = \hat{k}\cdot\hat{j}'$, where $\hat{k}$ and $\hat{j}'$ are unit vectors in the direction of the initial relative velocity and final diatom rotational angular momentum, respectively. If $x = \cos\chi$,

$$\frac{d\sigma_R}{d(\cos\chi)} = \sigma_R\cdot g(x),$$

(17)

$$\text{var}\left[\frac{d\sigma_R}{d\cos\chi}\right] = \left(\frac{N - S_{N_\alpha}}{NS_{N_\alpha}}\right)[\sigma_R\cdot g(x)]^2 + \sigma_R^2\text{var}[g(x)].$$

(18)

This treatment is not limited to the above mentioned variables. The probability density function of any other dynamical magnitude can be represented in an entirely similar way.

The truncation of the polynomial series is addressed by performing the Smirnov–Kolmogorov statistical test.[31,35]

Bidimensional probability density functions can also be represented by series of polynomials, although with a considerable higher computational effort and larger uncertainties. The mathematical procedure is basically the same and has been given elsewhere.[30,33]

In addition to the standard calculation of trajectories yielding final coordinates and momenta, some batches containing only reactive trajectories have been recalculated. By recording as a function of time the values of magnitudes as the relative radial and angular energies, bending angles, distance of closest approach in both $D + H_2$ and $DH + H$ channels it is possible to characterize the short-lived complexes and determine what is called their *collision time* as indicated below (see Discussion).

III. RESULTS

Total reaction cross sections for the $D + H_2(v = 0, j = 0) \rightarrow HD(v') + H$ reaction are shown in Fig. 1 as a function of the collision energy. For the two final vibrational states considered ($v' = 0, 1$), the cross section has a threshold and then grows monotonically with increasing translational energy. Although the agreement between the QCT total cross sections and the quantum mechanical values of
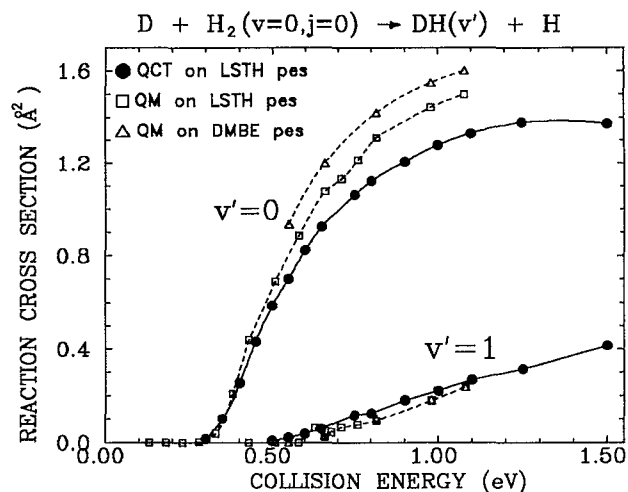

FIG. 1. Vibrational state resolved $v' = 0, 1$ integral reaction cross section as a function of the collision energy for the title reaction. Comparison with QM fully converged calculations: squares—Ref. 17 on the LSTH PES; triangles—Ref. 19 on the DMBE PES. Present QCT results (solid circles) on LSTH PES.

Zhang and Miller[17] [for the LSTH (Ref. 2) surface] and of Zhao *et al.*[19] [for the double many body expansion (DMBE) (Ref. 3) surface] was shown in previous work[31] to be acceptable, there are significant differences when cross sections resolved in the products vibrational states (v') are considered. The main difference are the systematically lower QCT values for $v' = 0$ as compared to both QM calculations,[17,19] the divergence being specially remarkable for values of the collision energy (E_T) higher than about 0.6 eV. This divergence with growing E_T might be due to "recrossing," which seems to be overestimated in the QCT calculation. The agreement in absolute value between QM and QCT cross sections is better for $v' = 1$. The difference between the two sets of quantum mechanical results is almost surely due to the different potential energy surfaces used for the calculations. Neither the quantum mechanical nor the classical curves show structure.

The (total) energy dependence of the reaction probability for this system for an initial value of the total angular momentum equal to zero ($J = 0$) is represented in Fig. 2, and also resolved in final vibrational states and compared to the QM results of Zhang and Miller.[17] At this level of resolution the QM results show a well known resonance structure with maxima and minima. This structure does not appear in the classical case, especially the first resonance at 0.95 eV is clearly absent in the QCT calculations. In an analogous way to the total cross sections just discussed, the QM reaction probability for zero impact parameter and for the ground vibrational state of the HD product ($P_{0 \leftarrow 0,0}^{J=0}$) is larger than the corresponding classical one. The quantum mechanical threshold for the production of $HD(v' = 1)$ is higher than the QCT one, due to the fact that classical trajectories ending with less energy than $v' = 1$ are assigned to this level by the "boxing" procedure (see above). If reactive trajectories ending with HD vibrational energy below $v' = 1$ were not counted in this channel,
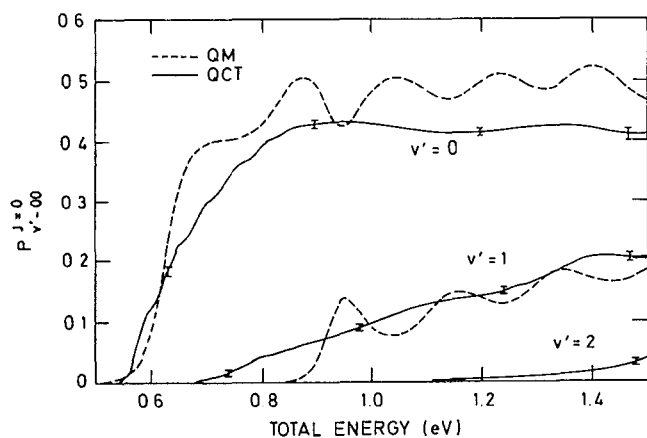
FIG. 2. Reaction probability at zero total angular momentum summed on j' for $v'=0$, 1, 2 as a function of the total energy. Solid line with error bars, present QCT calculations; dashed line, QM results by Zhang and Miller (Ref. 17), both on the LSTH potential energy surface.

FIG. 4. State resolved differential cross section at the collision energy $E_T=0.55$ eV for $v'=0$, $j'=0-7$. Error bars are shown for each curve indicating the most probable error of each fit.

the same threshold for $P^{j'=0}_{1\leftarrow0,0}$ would be the same in both QCT and QM.

The resolution of the reaction probability with total energy into final rotational states $P^{J=0}_{0,j'\leftarrow00}$ (see Fig. 3) shows that the classical results also exhibit a structure with broad maxima and minima. The curve for the $j'=1$ case can be approximately compared with the analogous QM curve for $H+H_2(v=j=0)\rightarrow H_2(v'=0,\ j'=1)+H$ calculated by Miller and Zhang [see Fig. 3(a) of Ref. 22]. Both curves correspond to different isotopic variants, and the comparison is just qualitative, but there are some features worth noting. The absolute value of the reaction probability is significantly smaller in the $D+H_2$ reaction. In both cases, there is a first broad maximum (centered at about 0.7 eV for $H+H_2$ and at 0.63 eV for $D+H_2$) followed by a broad minimum and an ulterior rise in the reaction probability. After this rise, the quantum mechanical curve shows a pronounced and relatively narrow "dip" corresponding to a well known resonance at a total energy at about 0.97 eV that has been assigned to the $(1,0,0)^{36-39}$ state of the H_3
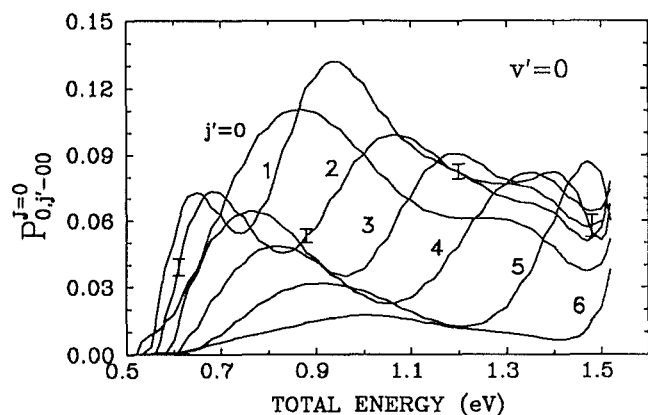

FIG. 3. Rotationally resolved reaction probability for $v'=0$, $j'=0-6$ as a function of the total energy at $J=0$. The error bars shown only for $j'=2$, give an idea of the statistical uncertainties (68%) of the calculations.
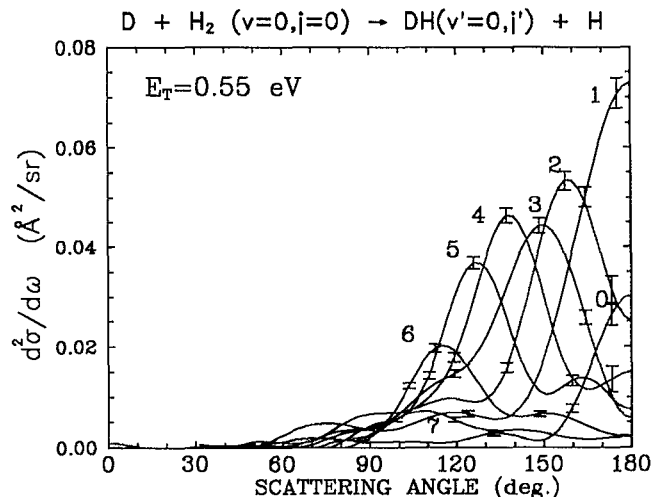
intermediate, where the conventional $(v_1,v_2^{\Omega_1}v_3)$ labeling of the vibrational levels of a linear triatomic molecule[40] has been adopted. The classical calculations show no sharp structure at this point. As already discussed in the Introduction, this sharp quantum mechanical resonance structure survives the summation in j' (see Fig. 2), but disappears when summing over the values of J (total angular momentum) relevant for a comparison with experiment. However, the "broad resonance" identified by Miller, Zhang, and Continetti[21,22] is caused by the evolution with J and E (total energy) of the first broad maximum,[22] which is also present in the QCT results (see below).

In order to increase the level of detail, and with the possibility of experimental resolution, we have calculated rotationally (j') state resolved differential cross sections for $E_T=0.55$ and 1 eV. The results are shown in Figs. 4–6. Figure 4 ($E_T=0.55$ eV, $v'=0$) can be compared to the quantum mechanical results of Zhang and Miller (see Fig. 21 of Ref. 17) and of Zhao et al. (see Fig. 6 of Ref. 19). The systematic evolution of these differential cross sections is similar in QCT and QM; the predominantly backward scattering characteristic of low j' becomes more sideways with increasing j'. The classical calculations yield distributions which are, in general, narrower and more sideways peaked than the corresponding quantum mechanical ones. It is interesting to point out that the scattering for low j' ($j'\leqslant2$) is not strictly constrained to the backward hemisphere, but presents a long tail, even a bump, at lower angles.

Figure 5 shows the same results but for $E_T=1$ eV, $v'=0$, and can be directly compared to Fig. 22 of Ref. 17 and Fig. 9 of Ref. 19. Here again, as indicated previously in the discussion of the total cross section (see Fig. 1), the QCT absolute values are lower by 10%–15% than the quantum mechanical ones. The final rotational distributions that can be inferred from the present differential cross sections are hotter by one or two quanta than the corre-
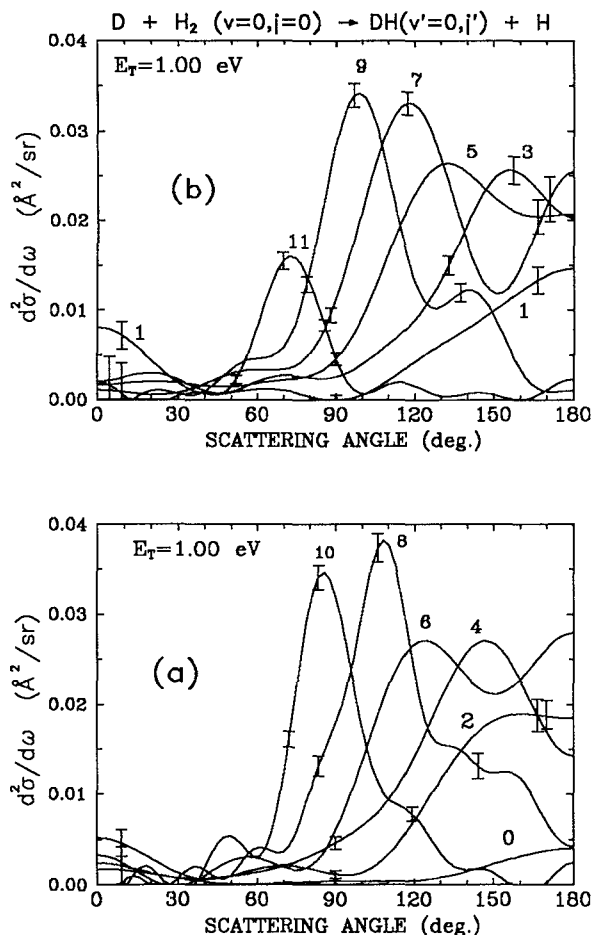
D + H₂ (v=0,j=0) → DH(v'=0,j') + H

FIG. 5. Same as Fig. 4 but for $E_T = 1.00$ eV, $v' = 0$. For clarity even j' (a) and odd j' (b) are displayed in separate graphs.

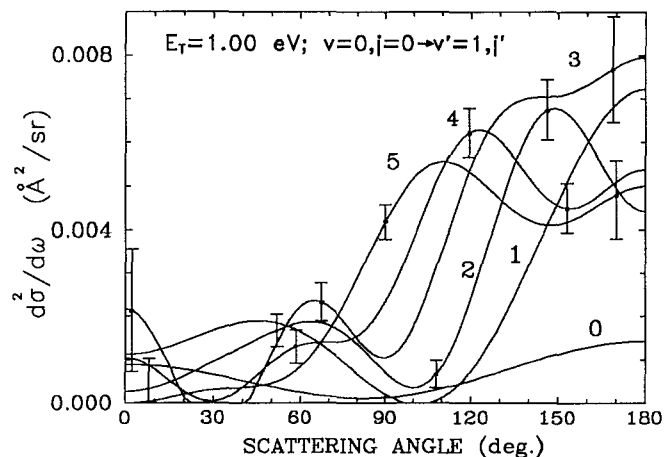FIG. 6. State resolved differential cross section for $v' = 1$, $E_T = 1.00$ eV, $j' = 0$–5. Error bars as in Figs. 4 and 5.

sponding QM ones, as already shown in previous works.[41,42] In spite of these differences, the systematic trend is again very similar in both QM and QCT calculations: low j' HD products give rise to essentially backward

scattering but with long tails extending to forward angles in similarity with the results of Zhang and Miller.[17] HD product molecules with higher j' appear at lower angles showing a sidewards behavior of relatively narrow range [full width at half maximum (FWHM) ~30°–40°]. The angular distributions of these high j' molecules have shoulders or tails extending toward $\theta = 180°$, but they die out quickly at low angles ($\theta \leqslant 30°$), so that the forward scattering is entirely due to HD molecules with low j'.

Figure 6 displays the differential cross sections for the production of HD($v' = 1$) molecules at a collision energy of 1 eV. This figure can also be compared with the quantum mechanical results of Zhang and Miller (see Fig. 23 of Ref. 17). The agreement is also very good in shape and closer in absolute value. In general, the angular distributions (from both QCT and QM) are broader than in the $v' = 0$ case, the forward component is less important and also for the higher j' they tend to die out at lower angles.

In general, there is an acceptable concordance between the above mentioned angle resolved TOF measurements[25,26] and the QM differential cross sections, although the best fit to the experimental data is obtained with a higher rotational excitation of the HD molecules scattered in the backward hemisphere. No simulation of the experiments has been attempted with the present QCT results, however given their similitude with the QM calculations the agreement with experiment is expected to be of the same order.

It has been often argued that part of the disagreement between QCT and QM state to state cross sections is due to the artificial partition in bins used to assign the quantum states of the molecules, and several procedures have been suggested in order to improve the agreement between the classical and quantum mechanical results. [See for instance the recent work by Mandy and Martin[43] in which they make use of microscopic reversibility and calculate indirect trajectories from H₂(0,j')+H back into the reagents' channel H+H₂(0,0). They find a better concordance between indirect QCT and QM calculations specially close to the threshold for the production of a given j'.] However, as in former works,[31,42] we have used the conventional partition in "boxes" (see Sec. 2) for the assignment of final states.

Figure 7 shows the reaction probability for the production of HD in a given j' state as a function of orbital (L), in this case also total (J), angular momentum for $E_T = 1$ eV. The correspondence with the just shown differential cross section is very clear. As expected, low j' are due to low L and high j' correlate with high L, note however that in the case of low j' there is a tail that extends up to the limiting L value for reaction and is responsible for the forward scattering commented on above.

Differential cross sections for the D+H₂($v=0$, $j=0$)→HD($v' = 0$, $j' = 2$)+H reaction are shown in Fig. 8. The $j' = 2$ case has been chosen because of its better statistics as compared with $j' = 0$ or $j' = 1$. The differential cross sections have in all cases a maximum in the backward direction with respect to the incoming D atom, and they broaden with increasing translational energy. Most inter-
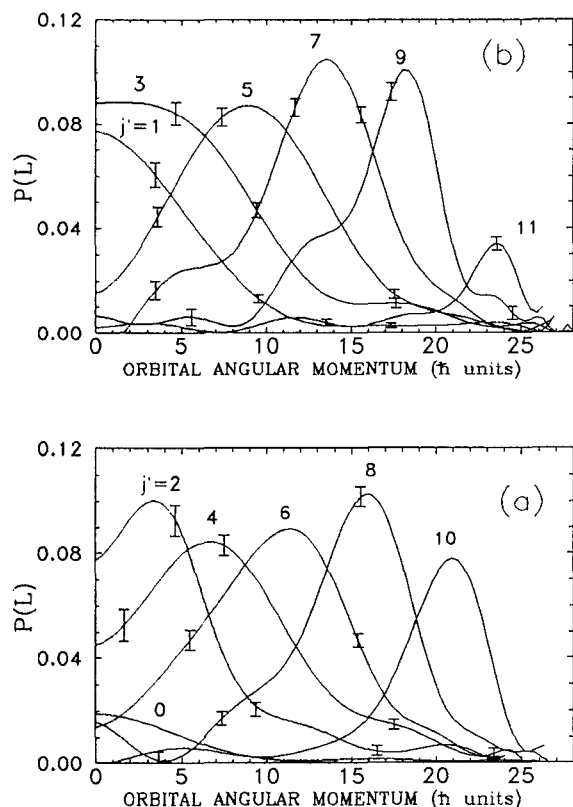
FIG. 7. Reaction probability as a function of the orbital angular momentum (here also total) at $E_T = 1.00$ eV for $v' = 0$, $j' = 0-11$. As in Fig. 5, even (a) and odd (b) j' are shown in separate panels for clarity.

FIG. 8. Solid angle differential cross section for $v' = 0$, $j' = 2$ at the indicated collision energies. Notice the "bump" in the 120°-60° region for low E_T values (a) that moves towards higher θ as E_T increases, becoming a forward peak (b) for $E_T \geqslant 1.00$ eV.

esting is, however, the small shoulder or bump appearing in all cases at the low angle side of the distribution. This bump shifts in the forward direction with growing collision energy.

Three dimensional representations of the differential cross sections as a function of scattering angle and of total energy are shown in Fig. 9 for $v' = 0$, $j' = 1$, 2, 3, 4 and the sum of all j', and for $v' = 1$ summed on j'. These plots of the differential cross section to the lowest specific j' states exhibit a ridge along the $E-\theta$ plane that extends from $E \sim 0.7$ eV, $\theta \sim 90°$ toward the region of high E and low θ. The ridge structure disappears for $j' > 4$. Summation over j' also destroys the observed structure. It can be seen in Fig. 9(e) and 9(f) for $v' = 0$ and $v' = 1$ summed over j' that the backward peak in the differential cross section is an oscillating function of energy. This fact was pointed out in the QM results of Zhang and Miller (see Fig. 24 of Ref. 17) and also confirmed in very detailed QCT calculations by Kornweitz, Persky, and Baer.[44]

The reaction probabilities as a function of L at the indicated total energies corresponding to the differential cross sections of Fig. 8 are represented in Fig. 10. This representation is analogous to the one reported by Miller and Zhang (Fig. 5 of Ref. 22) for the $H + H_2(v=0, j=0) \rightarrow H_2(v'=0, j'=0) + H$ reaction. In both cases there is a bump shifting to higher L values with increasing total energy. A 3D plot of the reaction probability vs total an-
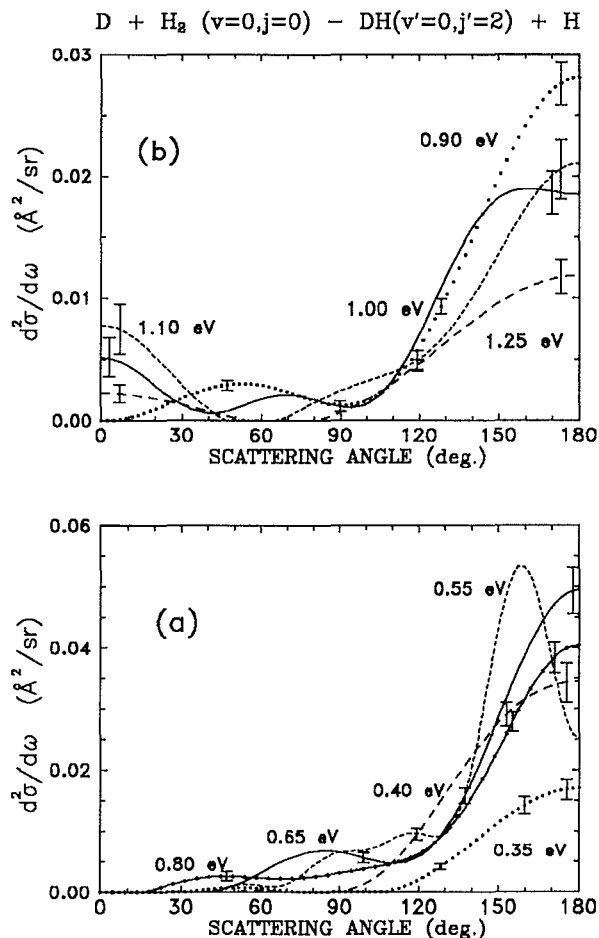
gular momentum and E (not shown here) exhibits a ridge structure[24] similar to the one found by Miller and Zhang.[22]

This behavior in both the angular distributions and in the reaction probabilities[21,22] has been attributed by the mentioned authors to the manifestation of a broad scattering resonance.

It is interesting to consider the evolution of the local QM maxima in $P(E,J)$[21,22] in the $E-J$ plane, i.e., the variation of the energy of this maximum with the total angular momentum, which is also the rotational quantum number of the hypothetical three atomic complex. The dependence of the energy of the local maximum E_m on $J(J+1)$ is approximately linear; and leads for the $D + H_2$ case[21] to an effective rotational constant of the complex $B_c \sim 8$ cm^{-1} (the rotational constant for an assumed linear D–H–H intermediate at the transition state is $B_c \simeq 7$ cm^{-1}). The intercept of this straight line (i.e., the energy of the local maximum when $J=0$) is $E_0 \simeq 0.74$ eV.

It is noteworthy that the classical result is again qualitatively similar to the QM one, showing also a linear dependence of $L(L+1)$ of the maxima vs total energy (in this case $L=J$). However, the corresponding rotational
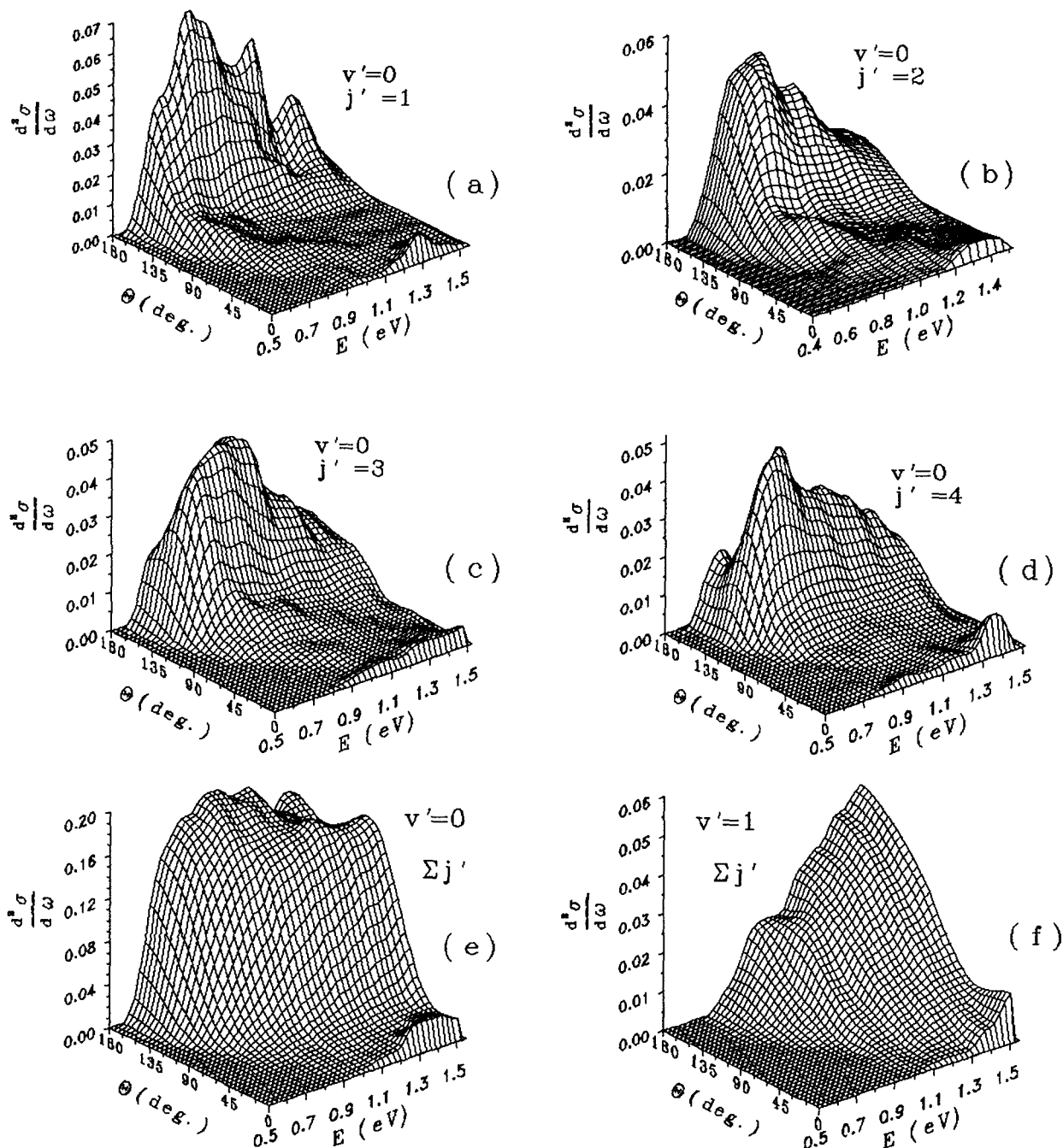
FIG. 9. Three dimensional plots of the solid angle differential cross section as a function of the scattering angle and total energy for $v'=0$ and $j'=1$ (a); $j'=2$ (b); $j'=3$ (c); $j'=4$ (d); $v'=0$ summed on j' (e) and $v'=1$ summed on j' (f).

constant for $j'=2$ is $B_c \simeq 14$ cm^{-1} and the intercept yields $E_0 \simeq 0.56$ eV.

IV. DISCUSSION

In a previous paper[24] we had shown that, for a given energy and for the lowest values of j', trajectories pertaining to the forward "tail" of the differential cross section and correspondingly to the larger angular momentum tails of the opacity function (i.e., the "ridge" in their energy evolutions) have longer "time delays" than the rest. Al-

though the duration of a collision (and hence the lifetime of a hypothetical collision complex) is in general an ill defined concept, several criteria have been used to evaluate this quantity. It is customary in quantum mechanics to estimate the lifetime of a collision complex from the width of an energy resonance via the Heisenberg uncertainty relation. In the classical case, the "time delay" is usually defined as "the limit as $R \rightarrow \infty$ of the difference between the time the particles spend within a distance R of each other and the time they would have spent there in the absence of
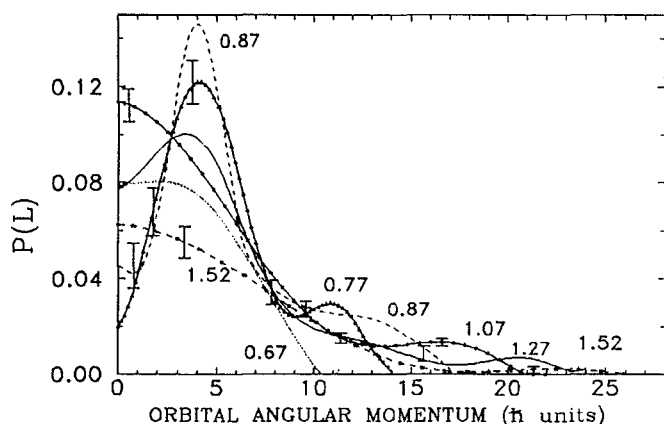
FIG. 10. Reaction probability vs orbital (also total) angular momentum for $v'=0$, $j'=2$ at the indicated total energies.

the interaction."[45] In our previous work we have computed the time delay for our $D+H_2$ reactive trajectories following Muga and Levine[23] as $\tau_{del}=T-R_f/v_{r_f}-R_i/v_{r_i}$ where T is the total duration of the trajectory initiated in channel i and ended in channel f, and R and v_r are the coordinate and the velocity of the atom–diatom relative motion at the initial and final times of the trajectory, where the atom–molecule interaction is assumed negligible.

The time delay calculated in this way is strictly valid for the comparison of the relative duration of collisions from a specific initial state to a fixed final state. However, when for a given initial state of the reactants the possible final states of the products have different energies (and hence different v_{r_f}) the bare comparison of their τ_{del} is not adequate as a measure of the relative collision duration. This is illustrated in Figs. 11–13 in which some characteristics of typical individual trajectories are depicted. The lower panels are conventional representations of the relevant $A+BC$ interatomic distances in the course of a reactive collision, R being the distance of the atom to the center of mass of the diatom. The upper panels show the simultaneous evolution of the potential energy V and of the relative radial energy $E_{rad,rel}$ as a function of time. The radial energy is calculated at the entrance as $P_R^2/2\mu_{D,H_2}$ and as $P_R'^2/2\mu_{H,HD}$ at the exit reactive channel, where P_R and P_R' are the conjugate momenta to R_{D,H_2} and $R_{H,HD}$. The middle panels refer to the variation of the bending angle $\alpha(\widehat{DHH})$ and of the angle of attack $\gamma(D-H_2)$, (where $\cos\gamma=\hat{r}\cdot\widehat{R}$; $\hat{r}$ and $\widehat{R}$ are unit vectors in the direction of the H_2 internuclear distance and R_{D,H_2}, respectively) during the trajectory. Figure 11 shows the typical case of a very direct trajectory. These trajectories are the most frequent for this reaction. As one would intuitively expect, the three nuclei stay together just for a very short time and the radial energy goes to zero only at one point, where the potential reaches its maximum. This is approximately the behavior one would expect for an interaction dominated by the repulsion from a hard sphere (in fact the angular distributions for this reaction have been modeled in this way[46,47]). The time delay for this trajectory has been calculated to be -11 fs; graphically, it can be obtained
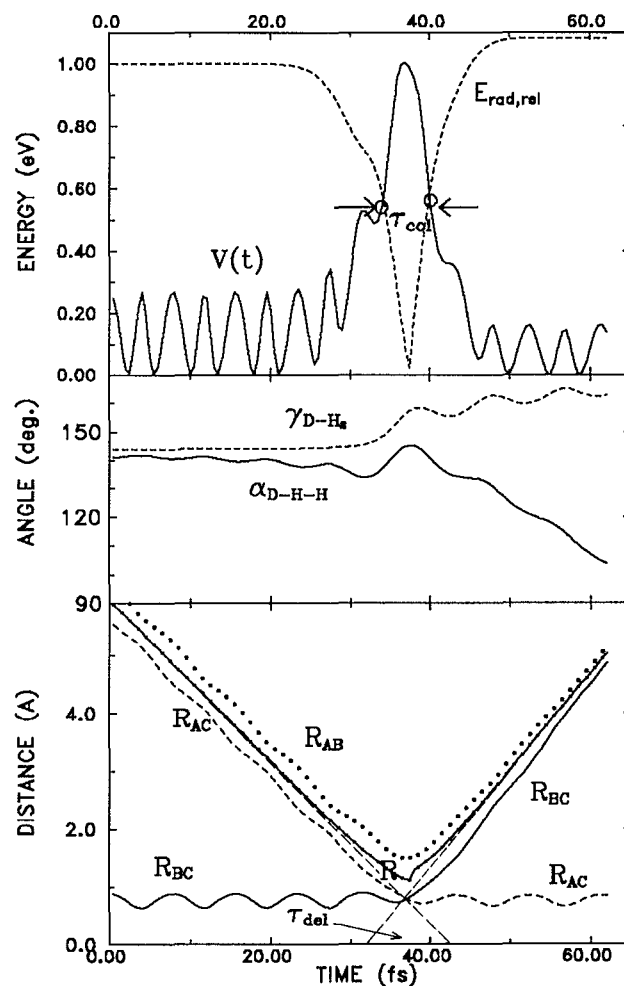

FIG. 11. Representation, as a function of time, of several magnitudes for an individual reactive trajectory at $E_T=1$ eV, $v'=0$, $j'=2$. Lower panel: interatomic distances R_{AB}, R_{BC}, R_{AC} and atom center of mass of the diatom distance R. The time delay, $\tau_{del}=-11$ fs, is shown, and can be graphically obtained as the difference between the intercepts of the asymptotic $R(t)$ lines after and before the collision with the time axis. Middle panel: bending $\alpha(DHH)$ and attack $\gamma(D-H_2)$ angles (see text). Upper panel: potential energy V and relative radial energy $E_{rad,rel}$. The collision time, $\tau_{col}=6$ fs, is defined as the time during which the radial energy is lower than the potential energy. Notice that the short duration of the collision is characteristic of a direct interaction.

from the extrapolation of the R dependence with time after and before the collision. The fact that these two lines intersect is an indication that the time delay is negative as expected for a direct and mainly repulsive interaction.

Figure 12 shows a typical "ridge" trajectory, with a longer, even positive time delay (~ 6 fs) and corresponding to a low value of j'. In the course of this trajectory the three nuclei remain at a closer distance and the radial energy approaches zero for an appreciably longer time than in the former case, i.e., a short-lived complex is formed in the course of the collision.

Figure 13 is the representation of a trajectory leading to HD in a high rotational state with a negative time delay ($\tau_{del}=-1.4$ fs). However, when looking at the lower and upper panel of this figure it is evident that the three atoms

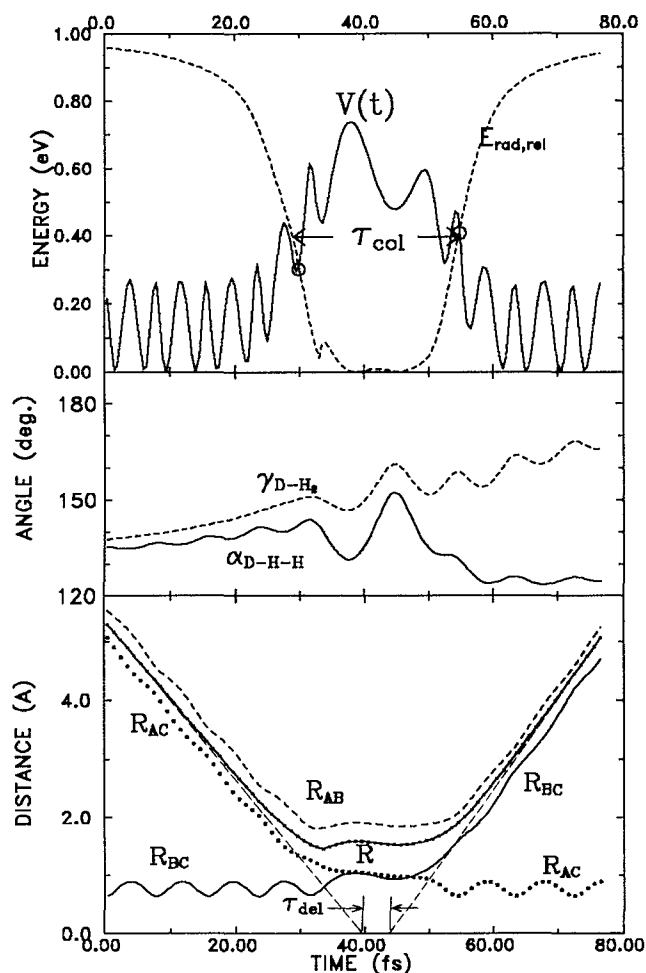FIG. 12. Same as Fig. 11 but for $E_T = 1$ eV, $v' = 0$, $j' = 1$. This case corresponds to a typical "ridge" trajectory leading to a short-lived complex, $\tau_{col} = 25$ fs, $\tau_{del} = 6$ fs.

FIG. 13. Same as Fig. 11 but for $E_T = 1$ eV, $v' = 0$, $j' = 9$. This is also a complex forming trajectory, $\tau_{col} = 27$ fs, but for high j'. Notice that, $\tau_{del} = -1.4$ fs, is in this case negative even when τ_{col} is similar to the one of the trajectory represented in Fig. 12 (see text).

stay at a close distance, and the radial energy remains close to zero for a time similar to that of the trajectory portrayed in Fig. 12, i.e., this trajectory also reflects the formation of a short-lived complex. The negative time delay is caused by the lower recoil velocity v_{rf} associated with the higher rotational excitation of the product molecule. In addition, the relation between τ_{del}, which is often negative, and the "lifetime" of the collision complex, loosely understood as the time the three particles hold together, is not straightforward.

For these reasons, we have preferred to define a "collision time" τ_{col} as the time during which the radial energy is lower than the potential energy, which is strongly perturbed as long as the three atoms stay in a close neighborhood (see Figs. 11–13). This definition is somewhat arbitrary, but is intuitive and independent of the final state of the molecule. Besides, when the spread in the relative velocities of the final states (v_{rf}) is relatively small, as is the case for the ridge trajectories, which are limited to low j', the correlation between τ_{col} and τ_{del} is very good. A linear representation of time delay vs collision time for the reactive trajectories corresponding to $E_T = 1$ eV, $v' = 0$, $j' \leqslant 3$
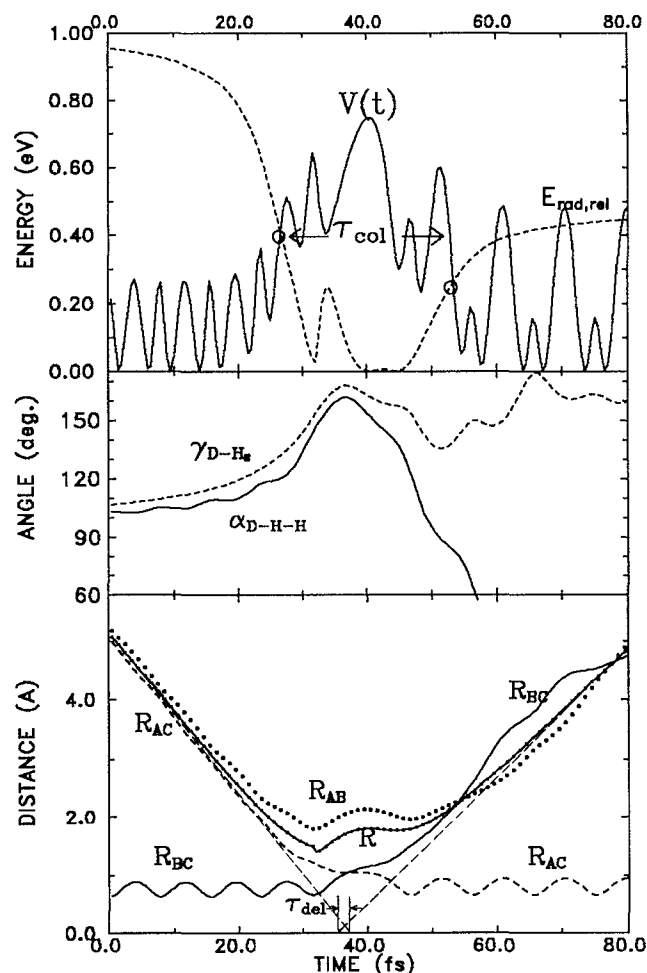
yields a slope of 0.94 and an intercept of -18.6 fs, a similar good correlation is found for all energies. In the following we will limit our discussion to "collision times" τ_{col} and will assume that τ_{col} is an approximate measure of the "lifetime" of the eventual collision complexes.

The present QCT calculations exhibit also examples of "trapped" trajectories, as the ones found by Muga and Levine[23] with positive and high time delays related to complexes with relatively long lifetimes (over 40 fs). However, these trajectories are not frequent enough to have a significant contribution in the observables of the collision. Besides, they are spread over the whole range of impact parameters and scattering angles.

Figure 14 represents the collision times as a function of scattering angle and of impact parameter for the lower [Figs. 14(a) and 14(c)] and higher [Figs. 14(b) and 14(d)] j' values at a collision energy E_T of 1.00 eV (qualitatively similar results are obtained for the rest of the energies). For both sets of j' values, one can see a wide distribution of collision times that range from very direct trajectories ($\tau_{col} \leqslant 10$ fs) to trajectories giving rise to short-
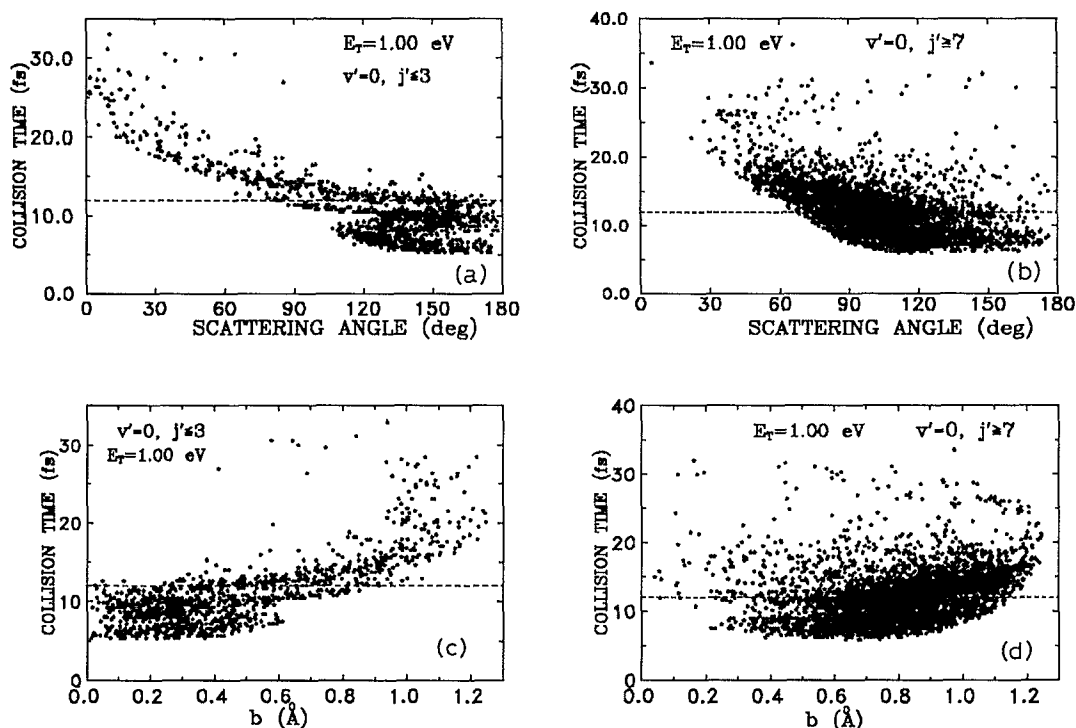
FIG. 14. Collision time as a function of scattering angle and impact parameter for reactive trajectories at $E_T = 1.00$ eV, (a) and (c) for $j' \leqslant 3$, and (b) and (d) for $j' \geqslant 7$. Dashed lines are meant to separate approximately direct trajectories from the rest in the low j' case.

lived complexes ($\tau_{col} \sim 15$–35 fs, depending on E_T). The most interesting observation is probably the fact that for low j' there is a good correlation between collision times and both scattering angle and impact parameter, whereas collision times are rather widespread over the extent of impact parameters and scattering angles available to the outgoing products with high j' states. When looking at Figs. 14(a) and 14(c) in detail one can appreciate, loosely speaking, three regions: one with a dense concentration of points at the higher scattering angle (lower impact parameter) side corresponding to the smallest collision times and thus to direct trajectories, a second region of densely packed points showing a tendency to increasing collision times with decreasing scattering angle (or increasing impact parameter), and finally a region with disperse points with the longest collision times for the lowest scattering angle (largest impact parameter). There is of course a gradual evolution and not a clear cut between these three parts of the collision time distribution.

Figures 15 and 16 show the differential cross section and reaction probability for low j' resolved in collision times. It is clearly seen that the local maxima in the differential cross sections and reaction probabilities as a function of angular momentum are almost entirely due to the longest-lived trajectories. In fact as can be deduced from Fig. 14 as the collision time increases the products at low j' are constrained to progressively more forward scattering angles. Especially appealing is the fact that the forward scattering component for $E_T = 1$ eV, something in principle experimentally detectable, is caused by these short-lived complexes.
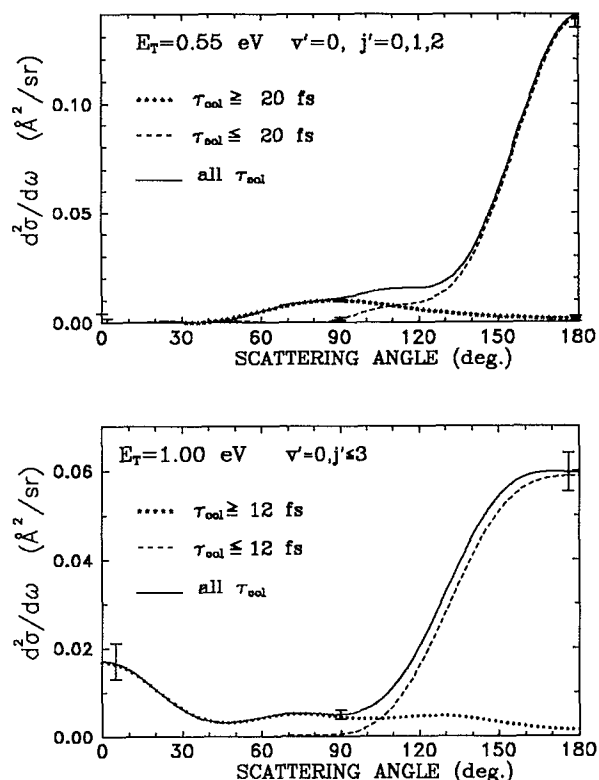

FIG. 15. Solid angle differential cross section for $E_T = 0.55$ eV, $v' = 0$, $j' = 0$–2 (upper panel); $E_T = 1$ eV, $v' = 0$, $j' \leqslant 3$ (lower panel). In both cases the contributions of trajectories with "short" and "long" collision times are separated. The border between "short" and "long" τ_{col} is chosen to be 20 and 12 fs for $E_T = 0.55$ and 1 eV, respectively.
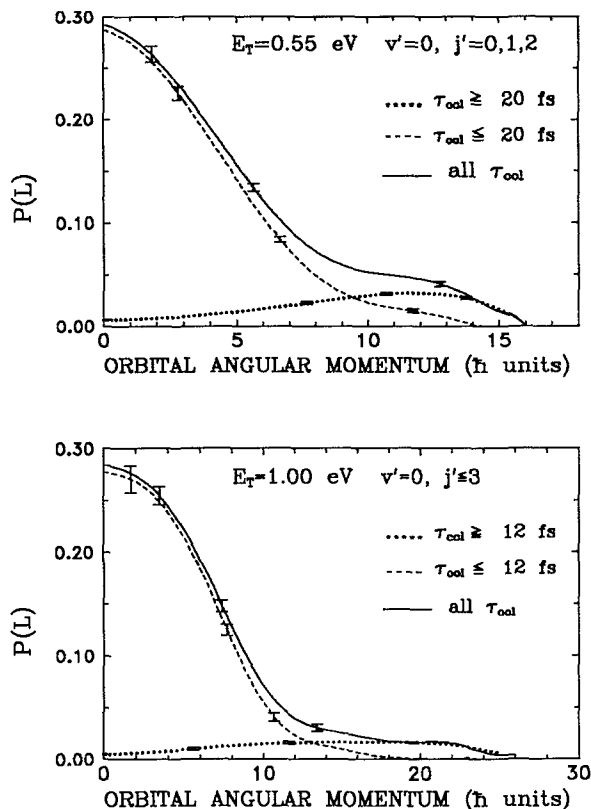
FIG. 16. Reaction probability as a function of the angular momentum at $E_T=0.55$ eV, $v'=0$, $j'=0-2$ (upper panel) and $E_T=1$ eV, $v'=0$, $j'=0-3$ (lower panel). As in Fig. 15 the contributions of trajectories with "short" and "long" collision times are separated.

FIG. 17. Differential cross section as a function of cos χ, where χ is the polarization angle (see text), for $E_T=0.55$ eV, $v'=0$, $j'=0-2$ (upper panel) and $E_T=1$ eV, $v'=0$, $j'=0-3$ (lower panel) separating the contribution of trajectories with short and long τ_{col} as in Figs. 15 and 16.

Another dynamical observable that might give some hints on complex formation and is also accessible to experimental investigation is the polarization angle χ, i.e., the orientation of the final rotational moment $\hat{j}'$ with respect to the relative velocity vector $\hat{k}$.[34,48] In their QM calculations Miller and Zhang[22] show that the ridges are more distinct for $m'=\pm 1$ than for $m'=0$ at $j'=1$. Present QCT calculations show that for $D+H_2(v=0, j=0) \rightarrow HD(v'j')+H$ at low j', direct trajectories, which correspond mainly to low impact parameters, tend to conserve helicity. For such collisions the output vector $\hat{j}'$ is found to be perpendicular to the initial relative velocity direction $\hat{k}$. Accordingly, the distribution of polarization angles is expected to be narrow and to peak at about cos $\chi \simeq 0$. On the other hand, in the longer-lived trajectories, the complex can rotate something and the correlation between $\hat{k}$ and $\hat{j}'$ will be lost. This is just what is found. In the fastest (direct) trajectories there is a strong perpendicular orientation between $\hat{k}$ and $\hat{j}'$, whereas in the longer-lived trajectories belonging to the ridge, the distribution of $\hat{j}'$ becomes almost isotropic, see Fig. 17. These findings are again in agreement with the quantum mechanical result and show that the features attributed to resonances in j', m', are also present in the classical behavior of the polarization angle χ.

At this point it is interesting to observe that the lifetime of the complex responsible for the broad quantum
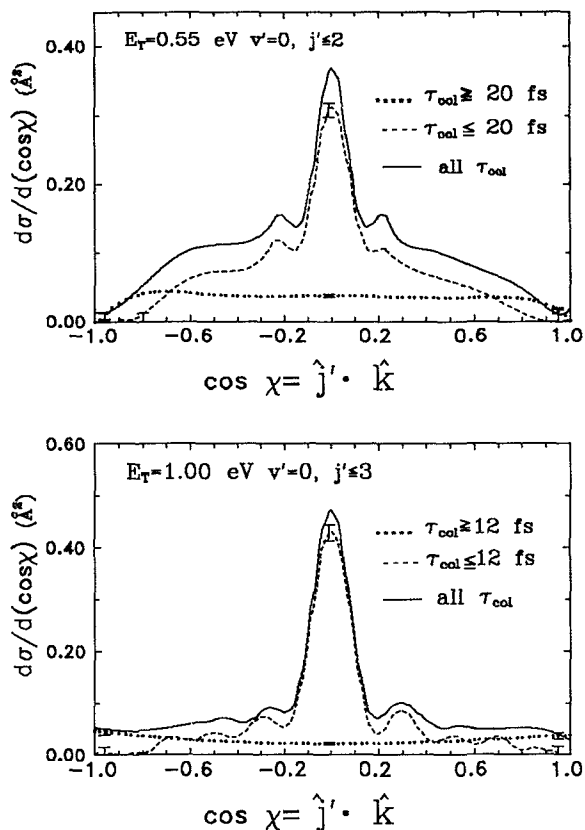
mechanical resonance commented on above can be estimated from its energy width Γ ($\tau_{Life} \sim \hbar/\Gamma$). This has been shown by Miller and Zhang[22] to be of the order of 0.15–0.25 eV, depending weakly on J. The corresponding lifetimes should thus be in the range 2–5 fs. In the classical picture this would not imply complex formation but rather very direct collisions (see Figs. 11–13). It should be recalled here that trajectories pertaining to the "ridge" have collision times between 15 and 35 fs, even larger than the lifetime estimated from the width of the well established quantum mechanical narrow resonance portrayed in Fig. 2 ($\tau_{Life} \sim 10$ fs). All this suggests that the ridge feature discussed throughout this article, might have a classical origin and not correspond to a pure quantum mechanical resonance.

The analysis of individual trajectories also provides information about the kind of relative motion the three atoms perform during the collision time τ_{col}. The middle panels of Figs. 11–13 show that complex forming trajectories, in contrast to direct trajectories, are characterized by ample angular movements during the collision. Both the bending angle α(DHH) and the angle of attack γ(D–H$_2$), which reflects predominantly an orbiting of the D atom around the center of mass of the molecule, undergo large variations when a short-lived complex is formed in the course of the collision. These bending or orbiting like
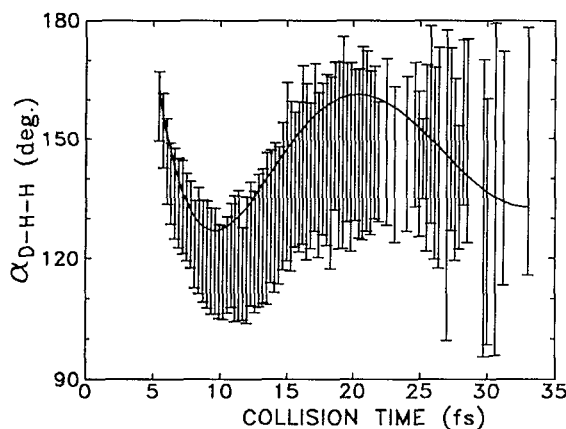
FIG. 18. The bars represent the range of variation of bending angles during the collision (see Figs. 11–13) vs the collision time for reactive trajectories at $E_T = 1$ eV, $v' = 0$, $j' = 0$–3. The solid line through the bars is a fit of the bending angle at the beginning of the collision ($E_{rad} = V$) as a function of collision time.

movements accompanying complex formation are demonstrated more rigorously in Fig. 18, that shows the range of variation of the bending angle α(DHH) in the course of the collision, as a function of τ_{col} for a series of trajectories at a relative energy $E_T = 1$ eV with $v' = 0$; $j' \leq 3$.

As expected, the most direct trajectories have a near collinear disposition at the begining of the collision; trajectories with a less favorable initial alignment can get reoriented (see Ref. 31 and references therein). The less collinear the attack the longer will be the collision time, but these trajectories can still be termed direct. From a certain value of τ_{col} the α(DHH) bending oscillations become much larger. These are the trajectories corresponding to short-lived complexes and are responsible for the ridge structure in the three dimensional representation of the differential cross section (see Figs. 9 and 15).

V. SUMMARY AND CONCLUSIONS

Extensive quasiclassical trajectory calculations for the $D + H_2(v=0, j=0) \rightarrow HD(v',j') + H$ reaction are presented here. A thorough comparison with exact quantum mechanical results has been performed in order to test further the level of detail to which classical mechanics can provide a good description of the dynamics of this reaction, and specially to discern the pure quantum mechanical effects from those also described by classical mechanics.

QCT vibrationally state resolved integral cross sections $\sigma_R(v')$ are similar to the ones obtained in exact quantum mechanical calculations; nevertheless for $v' = 0$, the quasiclassical cross sections are systematically lower (10%–15%) than the QM at the higher collision energies studied.

The total QCT reaction probability for $J=0$ as a function of energy ($P^{J=0}_{v' \leftarrow 0,0}$) is again a good approximation to the exact quantum mechanical one, although in the classical case the curves do not show the (resonance) structure characteristic of the quantum mechanical results. It is

however interesting to point out that the rotationally state resolved reaction probability ($P^{J=0}_{v',j' \leftarrow 0,0}$) calculated classically does show a structure with broad maxima and minima. The positions of these maxima and minima change gradually with j'.

At a deeper level of detail, QCT fully state resolved differential cross sections $[d^2\sigma(v',j')/d\omega]$ are in good agreement with the corresponding quantum mechanical ones showing the same systematic behavior as j' and E_T change. Specifically for low j', $d^2\sigma/d\omega$ show local maxima (bumps) that move with increasing energy toward lower angles. The representation of $d^2\sigma/d\omega$ in the plane formed by the total energy (E) and the center of mass scattering angle (θ) gives rise to a "ridge" structure similar but less pronounced than the one found in the quantum mechanical calculations and attributed to a broad resonance. The reaction probability as a function of angular momentum shows (also in analogy with the QM results) that there are local maxima at high values of the angular momentum for low j'.

It has been previously shown[24] that classical trajectories pertaining to the "ridge" in the three dimensional representation of $d^2\sigma/d\omega$ vs E and θ correspond to short-lived collision complexes. Here a *collision time* τ_{col} is tentatively defined as the time during which the radial energy is lower than the potential energy. This τ_{col} is shown to correlate very well with the conventional classical time delay τ_{del} for the trajectories relevant to the ridge. In terms of this collision time it is found that trajectories corresponding to the ridge lead to collision complexes that live for 15–35 fs, which represents a fraction of the three atomic rotational period, but is sensibly longer than the lifetime estimated from the width of the assumed QM broad resonance. The detailed analysis of individual trajectories indicates, contrary to our preliminary suppositions,[24] that large variations of the α(DĤH) bending angle take place during the complex forming collisions.

ACKNOWLEDGMENTS

[1] W. H. Miller, Annu. Rev. Phys. Chem. **41**, 245 (1990) and references cited therein.
[2] (a) P. Siegbahn and B. Liu, J. Chem. Phys. **68**, 2466 (1978); (b) D. G. Truhlar and C. J. Horowitz, *ibid.* **68**, 2466 (1978); **71**, 1514 E (1979).
[3] A. J. C. Varandas, F. B. Brown, C. A. Mead, D. G. Truhlar, and N. C. Blais, J. Chem. Phys. **86**, 6258 (1987).
[4] H. Buchenau, J. P. Toennies, J. Arnold, and J. Wolfrum, Ber. Bunsenges. Phys. Chem. **94**, 1231 (1990) and references cited therein.
[5] J. J. Valentini and D. L. Phillips, in *Advances in Gas Phase Photochemistry and Kinetics*, edited by N. M. R. Ashfold and J. E. Baggott (Royal Society of Chemistry, London, 1989), Vol. 2.
[6] D. G. Truhlar and A. Kuppermann, J. Chem. Phys. **52**, 3841 (1970).
[7] S. F. Wu and R. D. Levine, Chem. Phys. Lett. **11**, 557 (1971).
[8] G. C. Schatz and A. Kuppermann, Phys. Rev. Lett. **35**, 1266 (1975).
[9] G. C. Schatz, Annu. Rev. Phys. Chem. **39**, 317 (1988) and references therein.
[10] J. Z. H. Zhang and W. H. Miller, Chem. Phys. Lett. **153**, 465 (1988).

[11] J. C. Nieh and J. J. Valentini, Phys. Rev. Lett. **60**, 519 (1988); J. Chem. Phys. **90**, 1600 (1989).

[12] D. L. Phillips, H. B. Levene and J. J. Valentini, J. Chem. Phys. **90**, 1600 (1989).

[13] D. E. Manolopoulos and R. E. Wyatt, Chem. Phys. Lett. **159**, 123 (1989).

[14] J. M. Launay and M. Le Dourneuf, Chem. Phys. Lett. **163**, 178 (1989).

[15] D. E. Manolopoulos and R. E. Wyatt, J. Chem. Phys. **92**, 810 (1990).

[16] S. M. Auerbach, J. Z. H. Zhang, and W. H. Miller, J. Chem. Soc. Faraday Trans. **86**, 1701 (1990).

[17] J. Z. H. Zhang and W. H. Miller, J. Chem. Phys. **91**, 1528 (1989).

[18] N. C. Blais, M. Zhao, D. G. Truhlar, D. W. Schwenke, and D. K. Kouri, Chem. Phys. Lett. **11**, 166 (1990).

[19] M. Zhao, D. G. Truhlar, D. W. Schwenke, and D. J. Kouri, J. Phys. Chem. **94**, 7074 (1990).

[20] D. A. V. Kliner, D. E. Adelman, and R. N. Zare, J. Chem. Phys. **94**, 1069 (1991).

[21] R. E. Continetti, J. Z. H. Zhang, and W. H. Miller, J. Chem. Phys. **93**, 5356 (1990).

[22] W. H. Miller and J. Z. H. Zhang, J. Phys. Chem. **95**, 12 (1991).

[23] J. G. Muga and R. D. Levine, Chem. Phys. Lett. **162**, 7 (1989).

[24] F. J. Aoiz, V. J. Herrero, and V. Sáez Rábanos, J. Chem. Phys. **95**, 7767 (1991).

[25] (a) S. A. Buntin, C. F. Giese, and W. R. Gentry, J. Chem. Phys. **87**, 1443 (1987); (b) S. A. Buntin, C. F. Giese, and W. R. Gentry, Chem. Phys. Lett. **168**, 513 (1990).

[26] R. E. Continetti, B. A. Balko, and Y. T. Lee, J. Chem. Phys. **93**, 5719 (1990).

[27] (a) L. Schnieder, K. Seekamp-Rahn, F. Liedeker, H. Steuwe, and K. H. Welge, Faraday Discuss. Chem. Soc. **91**, 259 (1991); (b) L. Schnieder, Ph.D. Thesis, Universität Bielefeld, 1991.

[28] M. J. J. Vrakking, A. S. Bracker, and Y. T. Lee, *XIII International Symposium on Molecular Beams*, Books of abstracts (El Escorial, Madrid, Spain 2–7, June 1991), pp. 1–4.

[29] M. Karplus, R. N. Porter, and R. D. Sharma, J. Chem. Phys. **43**, 3259 (1965).

[30] D. G. Truhlar and J. T. Muckermann, in *Atom–Molecule Collision Theory*, edited by R. B. Bernstein (Plenum, New York, 1979), p. 505.

[31] F. J. Aoiz, V. J. Herrero, and V. Sáez Rábanos, J. Chem. Phys. **94**, 7991 (1991).

[32] D. G. Truhlar, B. P. Reid, D. E. Zurawski, and J. C. Gray, J. Phys. Chem. **85**, 786 (1981).

[33] F. E. Budenholzer, S. C. Hu, D. C. Jeng, and E. A. Gislason, J. Chem. Phys. **89**, 1958 (1988).

[34] D. A. Case and D. R. Herschbach, J. Chem. Phys. **64**, 4212 (1976).

[35] W. P. Press, B. P. Flannery, S. A. Teulosky, and W. T. Vetterling, *Numerical Recipes* (Cambridge University, Cambridge, 1988).

[36] B. C. Garrett, D. W. Schwenke, R. T. Skodje, D. Thirumalai, T. C. Thomson, and D. G. Truhlar, in *Resonances* edited by D. G. Truhlar (American Chemical Society, Washington, 1984).

[37] E. Pollack, R. W. Wyatt, J. Chem. Phys. **81**, 1801 (1984).

[38] M. C. Colton and G. C. Schatz, Chem. Phys. Lett. **124**, 256 (1986).

[39] J. M. Bowman, Chem. Phys. Lett. **124**, 260 (1986).

[40] G. Herzberg, *Molecular Spectra and Molecular Structure. II Infrared and Raman Spectra of Polyatomic Molecules* (Van Nostrand, New York, 1945).

[41] N. C. Blais and D. G. Truhlar, J. Chem. Phys. **88**, 5457 (1988).

[42] F. J. Aoiz, V. Candela, V. J. Herrero, and V. Sáez Rábanos, Chem. Phys. Lett. **161**, 270 (1989).

[43] M. E. Mandy and P. G. Martin, J. Phys. Chem. **95**, 8726 (1991).

[44] H. Kornweitz, A. Persky, and M. Baer, J. Chem. Phys. **94**, 5524 (1991).

[45] F. T. Smith, Phys. Rev. **118**, 349 (1960).

[46] G. H. Kwei and D. R. Herschbach, J. Phys. Chem. **83**, 1550 (1979).

[47] R. Götting, H. R. Mayne, and J. P. Toennies, J. Chem. Phys. **85**, 6396 (1986).

[48] J. M. Alvariño and A. Laganà, J. Chem. Phys. **95**, 998 (1991).